Hindawi
Journal of Renewable Energy
Volume 2022, Article ID 2916191, 12 pages
https://doi.org/10.1155/2022/2916191

Research Article

DFT Studies of p-N,N-(Dimethylamino) Benzoic Acid with Para or Meta–Electron Withdrawing or Donating Moieties for Dye-Sensitized Solar Cells (DSSCs)

Osman I. Osman,[1,2] **Mohamed Yagoub Alalem**,[3,4] **Mahmoud Mohamed Ali**,[3] **Shaaban A. Elroby**,[1,5] **and Saadullah G Aziz**[1]

[1]*Department of Chemistry, Faculty of Science, King Abdulaziz University, P.O. Box 80203, Jeddah 21589, Saudi Arabia*
[2]*Department of Chemistry, Faculty of Science, University of Khartoum, P.O. Box 321, Khartoum 11111, Sudan*
[3]*Department of Chemistry, Faculty of Pure and Applied Sciences, International University of Africa, Khartoum, Sudan*
[4]*Department of Chemistry, Rabigh College of Science and Arts, King Abdulaziz University, P.O.Box 344, Rabigh, Saudi Arabia*
[5]*Chemistry Department, Faculty of Science, Beni-Suef University, Beni-Suef 62511, Egypt*

Correspondence should be addressed to Osman I. Osman; oabdelkarim@kau.edu.sa

Received 1 June 2022; Accepted 24 August 2022; Published 22 October 2022

Academic Editor: Jedrzej Szmytkowski

Solar energy is receiving considerable attention worldwide. Our contribution here focuses on fabricating p-N,N-(dimethylamino) benzoic acid (4-DMABA) donor-π-acceptor derivatives for use in dye-sensitized solar cells (DSSCs). The gas-phase and solvated 4-DMABA and some of its electron donating or withdrawing ortho or meta derivatives were studied theoretically. Density functional theory (DFT) and time-dependent DFT (TD-DFT) were applied to visualize their structural, molecular, photoelectrical, electronic, and photophysical parameters. The parameters for monitoring DSSC efficacies include HOMOs, LUMOs, energy gaps, wavelengths, oscillator strengths, light harvesting efficiencies (LHE), electron injection driving forces (ΔG_{inject}), regeneration driving forces (ΔG_{regen}), open circuit voltages (V_{OC}), and short-circuit current densities (J_{sc}).

1. Introduction

The rapid development and utilization of renewable energy are vital measures to provide clean energy sources. The steadily increasing global demand for energy, coupled with the depletion of harmful environmental effects, which are associated with the combustion of fossil fuels, has necessitated the rapid search for renewable energy sources [1]. At the present time, the global energy sources are mainly dependent on fossil fuels. This energy source is the main cause of global warming that brings about devastating climate changes as a result of the emitted carbon dioxide (CO_2) [2]. However, the alarming rate of depletion of the major conventional energy resources such as coal, petroleum, and natural gas, coupled with the environmental degradation caused by the process of harnessing these energy sources, has necessitated the investment in renewable energy resources that could provide sufficient power without degrading the environment through greenhouse gas emissions. These renewable energy sources include wind power, solar energy, hydropower, bioenergy, and geothermal energy.

Dye-sensitized solar cells (DSSCs) have received considerable attention due to their low-cost conversion of photovoltaic energy compared to the silicon-based semiconductor ones [3]. In particular, DSSCs are characterized by acquiring a wide bandgap semiconductor, typically titanium dioxide (TiO_2) that can be sensitized by molecular organic dyes. This architectural design, together with a transparent conductive oxide layer (TCO) and a redox electrolyte, typically iodide/triiodide, is capable of capturing light in the visible region of the spectrum [4].

Solar energy is considered the most promising renewable energy source for supplying the future with energy [5]. Consequently, dye-sensitized solar cells (DSSCs) have attracted ever-increasing attention in scientific research and in practical applications since the first report by O'Regan and Grätzel in 1991 [6] due to their low cost and high efficiency in converting sunlight into electricity. In DSSCs, the incoming light photons excite the dye electrons, which are injected into the conduction band of the nanocrystalline metal oxide. This step is followed by the regaining of electrons by the dye from the redox couple in the electrolyte solution [7]. Generally, a power-conversion efficient dye sensitizer has the following characteristics: The highest occupied molecular orbital (HOMO) energy must be below the conduction band minimum (CBM) of the semiconductor (TiO_2) and the lowest unoccupied molecular orbital (LUMO) energy should be higher than the energy of the redox electrolyte pair (I^-/I^{-3}).

The sensitizing dyes play important roles in DSSCs through maximizing the solar-to-electricity conversion efficiency [8]. In contrast to experimental results on metal-free organic dyes, the theoretical investigations are still lagging behind. Only a few research groups have studied the electronic structures and photophysical properties of the dye sensitizers [9] and the intramolecular electron dynamic process between dyes and TiO_2 nanocrystals [10, 11]. Wang et al. [11] have thoroughly studied theoretically 3-(10-butyl-8-(methylthio)-10H-phenothiazin-3-yl)-2-cyanoacrylic acid coupled with diketopyrrolopyrrole derivatives. In this context, the theoretical study of the structures of several benzoic acid derivatives has been conducted recently with considerable accuracy [12]. The structures of p-dimethylamino benzonitrile (pDMABN) [13], p-aminobenzoic acid (pANA) [14],and Ethyl-4-(dimethylamino) benzoate (4-EDMAB) were taken as references to study the effect of para-substituents on the aromatic-ring moiety. The structure of p-(dimethylamino) benzoic acid (hereinafter-DMABA), with the dimethylamino group as a para-substituent having relatively intermediate behavior as compared with the nitro and amino groups, is expected to yield more information about the cooperative electronic interaction in the para-substituted compounds.

In this study, we endeavor to monitor the characteristics of several donor-π-acceptor (D-π-A) dyes having $-N(Me)_2$ and –COOH moieties as donors and acceptors, respectively. The electronic structure and optical absorption properties of eight dye sensitizers (see Scheme 1) in the gas-phase and dimethyl sulphoxide (DMSO) were investigated by using density functional theory (DFT) and time-dependent density functional theory (TD-DFT). Based on the calculated results, we analyzed the role of the different electron-donor or–acceptor groups in tuning the geometries, electronic structures, and optical properties. In addition, we aim to see the effects of the donors or the acceptors of the sensitizers on the open circuit photovoltage (V_{oc}) and the short-circuit current density (Jsc) of the cell by discussing the key factors affecting V_{oc} and J_{sc} with the goal of finding potential sensitizers for use in solar cells.

2. Computational Details

The *ab initio* molecular orbital calculations were performed using the Gaussian09 suites [15] and viewed by GaussView software [16]. All calculations for structural optimization were done by density functional theory (DFT) [17] using the B3LYP (Beck three parameter Lee-Yang-Parr) [17], the Coulomb-attenuating Beck three parameter Lee-Yang-Parr (CAM-B3LYP) [18], the pure functional, Perdew, Burke, and Ernzerhof (PBEPBE) [19], and the long-range corrected hybrid ωB97XD [20] functional. All the geometrical structures of the substrates yielded global minima in their potential energy surfaces. This is achieved by performing vibrational calculations that gave no imaginary frequencies. The time-dependent density functional theory (TD-DFT) [21] was used to simulate the absorption and emission spectra of the substrates which were monitored by the Chemissian Software [22]. The effects of basis sets were investigated by using the triple-zeta without and with polarization and diffuse functions on hydrogen and heavy atom basis sets: 6-311G, 6–311++G, 6–311G**, 6–311+ G**, and 6–311++G** [23]. The HOMO and LUMO, electron absorption and emission spectra, oscillator strengths (f), and light harvesting efficiency of the optimized substrates were investigated using the same methods and basis set in the gas phase. The dimethyl sulphoxide (DMSO) solvated substrates were studied using the polarizable continuum model (PCM) [24] for simulating their absorption and emission spectra.

3. Result and Discussion

3.1. The Geometry. Table 1 lists some selected bond lengths, angles, and dihedral angles of the neat 4-DMABA and Ti^{+4}-bound complex computed by using PBEPBE, B3LYP, CAM-B3LYP, and WB97XD functionals with 6–311++G** basis sets in the gas phase. The atom numbering of these two substrates are shown in Figure 1, while their standard orientations are depicted in Tables S2 and S3. A quick look at Table 1 shows that the neat 4-DMABA estimated geometrical parameters using all DFT functionals are in excellent agreement with each other. The calculated exocyclic C1–N15 and C4–C11 bond lengths of 4-DMABA of *ca.* 1.377 and 1.471 Å, respectively, are in excellent agreement with those of its solid-state crystal structure; while the C11–O12 and C11–O13 bonds of the former are longer (*ca.* 0.04 Å) and shorter (0.09 Å), respectively, compared to those of the latter as a result of dimerization in the solid-state [25]. All DFT functionals have predicted completely planar gas-phase geometries, but the crystal structures have indicated deviations from a planarity of *ca.* 2–4° [25]. The exocyclic C1–N15 bond length is shorter than a typical C–N single bond by 0.094 Å [26] and longer than an exemplary C=N double bond by 0.105 Å [27]. Likewise, the exocyclic C4–C11 bond length is shorter than a model C–C bond length by 0.068 Å [28] and longer by 0.134 Å compared to a representative C=C double bond [29]. The multiple bond characters of these bonds are quite important in dictating the passage of charge from donors (N–N-dimethyl amine group) to acceptors (carboxyl moiety).

Table 1: Some selected bond lengths (Å) bond angles (°) and dihedral angles (°) of gas-phase 4-DMABA (D1) and 4-DMABA-$T^{+4}(OH)_4$ (D2) which were calculated by using B3LYP, CAM-B3LYB, PBEPBE, ωB97XD functionals, and 6–311++G** basis set.

Parameters	*B3LYP*		*CAM-B3LYB*		*PBEPBE*		*WB97XD*		Expt.*	Expt.#
	D1	D2	D1	D2	D1	D2	D1	D2		
C1–N15(14)	1.377	1.375	1.378	1.370	1.387	1.377	1.378	1.372	1.376	1.368
C4–C11	1.472	1.463	1.470	1.461	1.473	1.464	1.473	1.464	1.472	1.475
C11–O12	1.212	1.274	1.207	1.268	1.224	1.285	1.208	1.275	1.248	1.271
C11–O13	1.365	1.284	1.354	1.275	1.376	1.295	1.376	1.267	1.282	1.278
O12–C11–O13	121.2	116.2	121.2	116.2	121.3	116.6	121.4	116.6	121.9	119.2
C6–C1– N15 –C20(19)	−180	−175.2	−180	−177.2	−180	−176.5	−180	−173.5	−178	−178.3
O12–C11– C4–C3	180	179.5	180	179.2	−180.0	179.6	180.0	178.9	176	179.2

*Taken from Ref.26 #Taken from Ref.31.

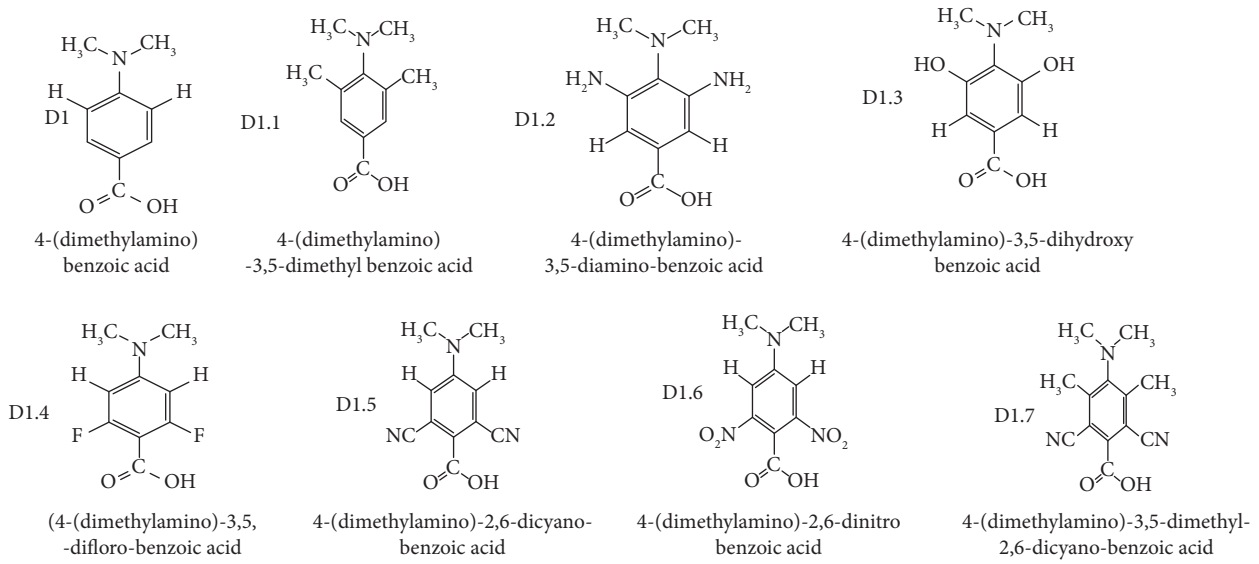

Scheme 1: 4-dimethyl amino benzoic acid (D1) derivatives (D1.1-D1.7).

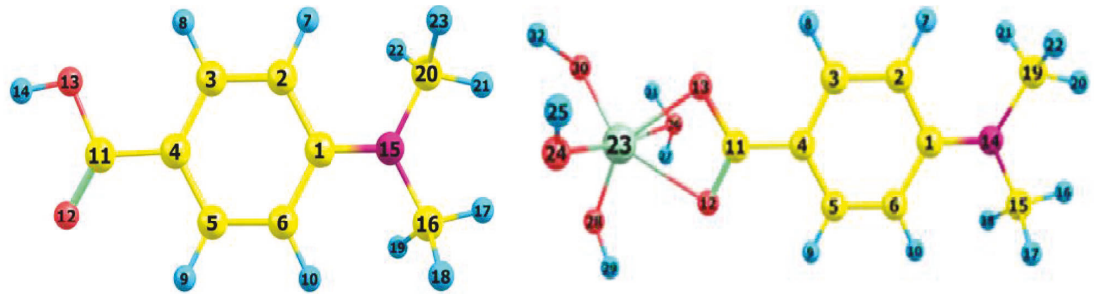

Figure 1: The atom numbering of the optimized structure of (a) 4-DMABA (D1) and (b) 4-DMABA-$T^{+4}(OH)_4$ (D2) chromophores.

In comparison, the calculated gas-phase geometrical parameters of the Ti^{+4}-bound complex using all DFT functionals are in complete coincidence with each other and agree satisfactorily with those of a DMABA-Zn bond complex [30] as shown in Table 1. Noticeably, the planarity of the neat dye is hardly lifted upon chelation with the titanium hydroxide. Here, again, the exocyclic C1–N15 and C4–C11 bonds have witnessed a slight shortening as a result of the bidentate binding of 4-DMABA with $Ti(OH)_4$. In addition, the parent dye O12–C11–O13 bond angle is closed by *ca.* 5° to facilitate the bidentate complexation. These observations could be harnessed as indicators for the existence of more charge transfer from the donor to the acceptor. As the charge transfer is a cornerstone in the functioning of solar cells; this parameter will be investigated more thoroughly in the upcoming sections.

3.2. Frontier Molecular Orbitals (FMO). The Frontier molecular orbitals (FMOs) include some of the lowest unoccupied molecular orbitals (LUMOs) and a few of the highest

occupied molecular orbitals (HOMOs). The HOMO-LUMO energy gap is an ideal quantum mechanical descriptor that plays a major role in governing a wide range of chemical interactions [31]. In Figure 2 are depicted the FMOs of the parent dye and its Ti^{+4}-bound complex were computed by using the B3LYP/6311++G** level of theory. As shown in Table 2, all the FMOs of the parent dye are stabilized upon chelation with $Ti(OH)_4$. The LUMO+2 for the neat dye is a π^*-antibonding orbital spreading all over the dye skeleton, while that of the Ti^{+4}-bound complex is crowding around the Ti-atom. The LUMO+1 is 0.07 and 0.24 eV below the LUMO+2 of the parent dye and its Ti^{+4}-boud complex, respectively. Both of them are benzene ring π^*-antibonding orbitals. The LUMOs are concentrated around the carboxylate chelating acceptor moiety as π^*-antibonding orbitals. The LUMO of the neat dye is stabilized by 0.74 eV upon chelation. The HOMOs of both species are π-bonding orbitals engulfing the donor dimethylamino group. The complexation effect has decreased the energy gap of the neat dye by 0.6 to 0.7 eV, which means more charge flow [32]. The HOMO-1 and HOMO-2 of the neat dye are oxygen atom's nonbonding orbitals and benzene π-bonding orbitals, respectively. Upon chelation, both of them characterize the π-bonding orbitals on the benzene moiety. They are 1.428 and 1.800 eV below the HOMO of the parent species, respectively: and 1.409 and 2.215 eV underneath the HOMO of the Ti^{+4}-bound complex, respectively.

As a conclusion, all the as-investigated functionals have yielded narrower energy gaps and larger dipole moments upon chelation, in excellent agreement with that of Wang et al. [11]. This means that an easy charge flow occurs when the dye preys on the Ti $(OH)_4$ molecule. It is apparent that the pure PBEPBE functional has given the straight energy gap and larger dipole moment; while the dispersion ωB97XD functional produced the colossal energy gap and smaller dipole moments. The order of decreasing energy gaps among the applied functionals is as follows: ωB97XD > CAM-B3LYP > B3LYP > PBEPBE [33]. This trend is inverted by the calculated dipole moments. The pure PBEPBE functional yielded the narrowest energy gap by stabilizing the LUMO and destabilizing the HOMO; while the ωB97XD functional gave the widest energy gaps through destabilizing the LUMO and stabilizing the HOMO [34]. As the hybrid B3LYP functional gave energy gap suitable for reasonable charge flow; it was adopted for simulating the absorption and emission spectra and the theoretical testing of DSSCs [35].

3.3. Electronic Excitations of 4-DMABA Derivatives. The $\pi \longrightarrow \pi^*$ and $n \longrightarrow \pi^*$ electronic transitions in π-conjugated organic compounds are recognized for leading to UV-visible spectra [36, 37]. Table 2 lists the maximum absorption wavelengths of gas-phase 4-DMABA dye (D1) using the as-investigated functionals with 6–311++G** basis set. The parent (D1) absorption UV-visible bands calculated by B3LYP functional are in excellent agreement with its experimental ones [38]. In Table S1 (Supplementary Information), the electronic transitions of D1 are registered using B3LYP and PBEPBE functionals with different basis sets. The polarization functions have a propensity to underestimate the maximum absorption wavelengths [39], while the diffuse functions are liable to overestimating them [40]. That is, when the polarization [6-311G**] and the diffuse [6–311++G] basis sets were applied with B3LYP and PBEPBE functionals, the maximum absorption wavelengths were blue-shifted and red-shifted, respectively, compared with the values obtained by using the 6-311G basis set with these two functionals (See Table S1). Hence, it is recommended to use both the polarization and diffuse functions in simulating UV-Vis spectra [41].

Normally, molecules with large dipole moments have strong asymmetric electronic charge distribution and thus become more reactive and sensitive to external electric fields [42]. The theoretical UV-visible spectra of 4-DMABA using TD-B3LYP and TD-PBEPBE functionals with a 6–311++G** basis set of theory are shown in Figures S1 and S2. TD-B3LYP/6-311++G** predicted intense electronic transition bands at $\lambda_{max} = 290$ nm ($f = 0.5297$) which is red-shifted by *ca.* 11 nm compared to the experimental value of 310 nm [11, 38]. The calculations showed that these bands originate mainly from a HOMO- > LUMO transition (See Table S1). Moreover, the computed dipole moment using this level of theory of 5.164 Debye is in line with the values of the predicted electronic bands (See Table 2).

We have also investigated some D1 derivatives (D1.1-D1.7) by replacing the hydrogen atoms at the ortho or meta positions by two or four CH_3, OH, NH_2, F, CN, and NO_2 as electron donating or withdrawing moieties (cf. Scheme 1). Figure 3 depicts their optimized geometries using the B3LYP/6-311++G** level of theory. Their standard orientations are registered in Tables S4–S10. Figure 4(a) depicts the absorption spectra of the DMSO-solvated D1-D1.7 dyes which have been simulated by using TD-B3LYP/6-311++G** level of theory.

Table 3 lists the calculated HOMO, LUMO, bandgaps, absorption wavelengths, oscillator strengths, light harvesting efficiencies (LHE), and electronic transition assignments of the gas-phase D1-D1.7 derivatives using the B3LYP/6-311++G** level of theory. On the one hand, the electron donating groups (CH_3, NH_2, and OH) at the ortho positions have widened the band gaps and hence blueshifted the wavelengths compared to those of the parent dye (D1). On the other hand, the electron withdrawing groups (F, CN, and NO_2) at the meta positions have straitened the bandgaps and accordingly redshifted the wavelengths [11]. When both electron donating (CH_3) and withdrawing (CN) ligands are used (D1.7); moderate results are obtained for both the band gap and absorption wavelength. These UV spectra originate mostly from HOMO to LUMO transitions.

In Table 4 are registered the HOMO, LUMO, bandgaps (ΔE), absorption and emission wavelengths, the emission oscillator strengths of D1.1–D1.7 solvated (DMSO ($\varepsilon = 46$)) derivatives which were obtained by using TD-B3LYP functional with 6–311++G** basis set. Apart from D1.4, all the energy gaps of the elected dyes (D1.1-D1.7) are smaller than that of the parent dye(D1).

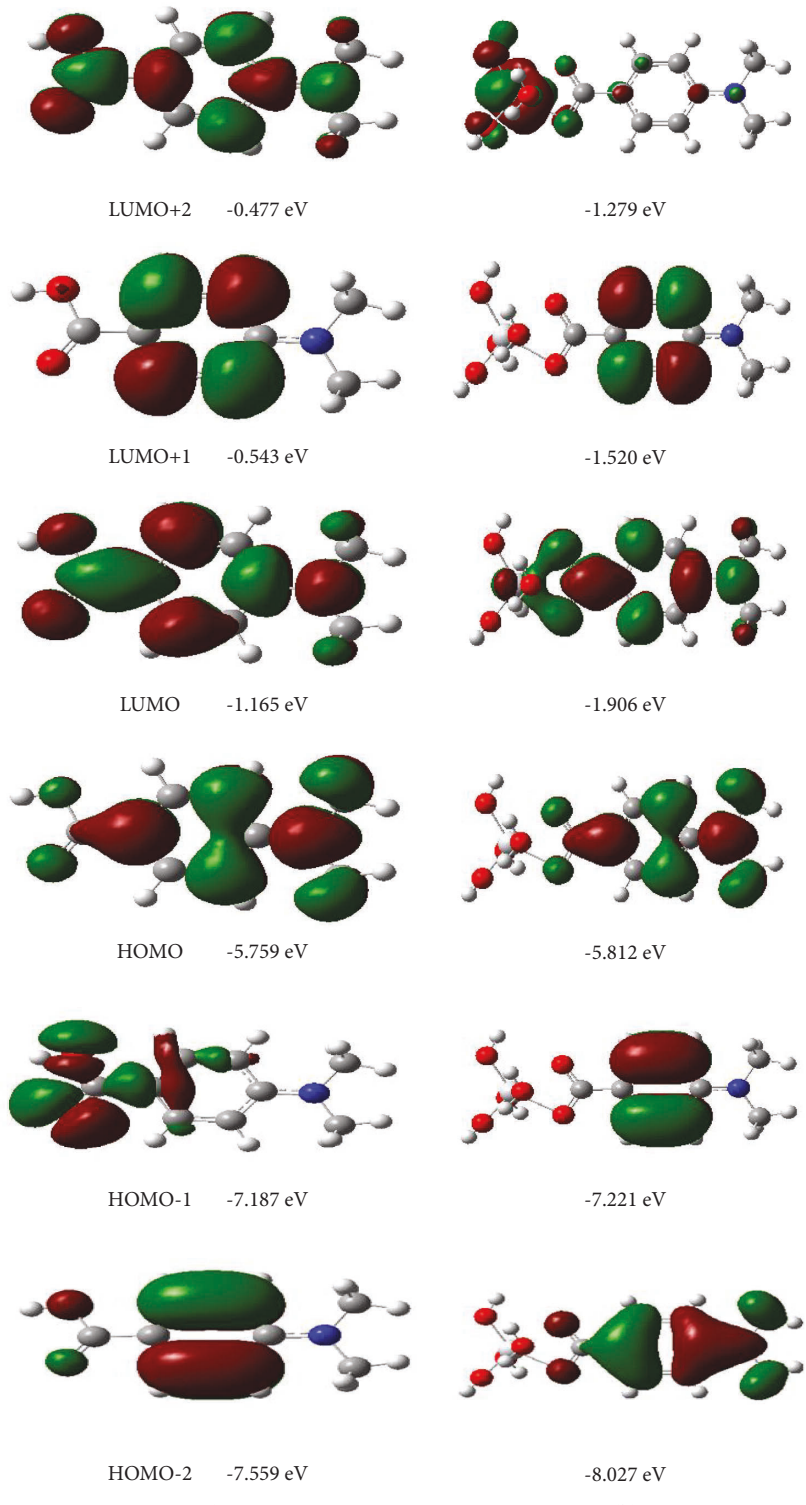

Figure 2: The Frontier molecular orbitals (FMOs) of (a) the neat 4-DMABA and (b) 4-DMABA-$T^{+4}(OH)_4$ which have been calculated by using the B3LYP/6-311++G** level of theory.

The derivatives D1.6, D1.7 and D1.5 gave the smallest energy gaps amongst them. The absorption wavelength (λ_{abs}/nm) of D1.1 to D1.7 derivatives are slightly shifted compared to that of D1. The absorption wavelength of the derivatives having–I (inductive) with +R (resonance) effects (NH_2, OH, and F) were generally blueshifted compared to that of the parent D1; while those for the ones with–I effect (CN) were redshifted. In the methyl

Table 2: The FMOs (eV), energy gaps (ΔE/eV), dipole moments (μ/Debye), and absorption spectra maxima (λ_{max}/nm) of the gas-phase neat 4-DMABA and 4-DMABA-$T^{+4}(OH)_4$ complex which was calculated by using different DFT functionals with 6–311++G** basis set.

Parameters	*B3LYP*		*CAM-B3LYB*		*PBEPBE*		*ωB97XD*	
	D1	D2	D1	D2	D1	D2	D1	D2
LUMO+2	−0.477	−1.279	0.583	0.094	−0.838	−1.966	1.260	0.715
LUMO+1	−0.543	−1.520	0.131	−0.057	−1.217	−2.222	0.858	0.597
LUMO	−1.165	−1.906	0.104	−0.486	−1.860	−2.592	0.751	0.157
HOMO	−5.759	−5.812	−7.067	−7.087	−5.006	−5.081	−7.580	−7.615
HOMO-1	−7.187	−7.221	−8.672	−8.682	−6.129	−6.418	−9.210	−9.222
HOMO-2	−7.556	−8.027	−9.359	−9.630	−6.366	−6.587	9.811	−10.123
ΔE	4.594	3.906	7.171	6.601	3.146	2.489	8.331	7.772
μ	5.164	6.277	4.883	5.829	5.356	6.686	4.822	5.705
λ_{max}	290.1	356.6	267.2	275.2	321.5	470.5	265.2	270.2

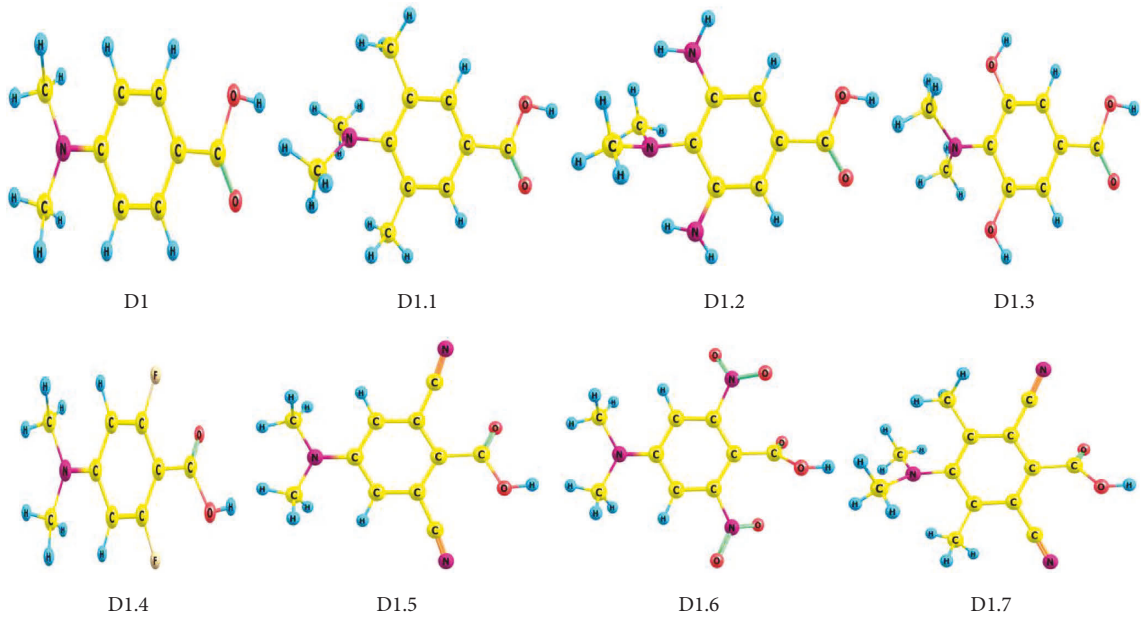

Figure 3: The optimized geometrical structures of 4-DMABA derivatives (D1-D1.7) have been obtained by using the B3LYP/6-311++G** level of theory.

derivative (D1.1), the methyl groups with +I effect have redshifted the peaks. Similar trends have been shown by the emission spectra.

Furthermore, the emission spectra of the DMSO-solvated dyes D1.1–D1.7 are depicted in Figure 4(b), while the corresponding values for the orbitals responsible for the first excited singlet state (HOMO-LUMO contribution), excitation energy (cm^{-1}), maximum emission wavelength (λ_{em}), emission oscillator strength (f), excited-state lifetime (τ), and Stokes shift (SS) are presented in Table 4. The emission spectra arising from the S_1–S_0 transitions were assigned $\pi^* \longrightarrow \pi$ character for all the studied dyes. Similar to the absorption spectrum, the emission bands were found to be related to the HOMO-to-LUMO transitions. It is noteworthy that the small values of the Stokes shift (SS) were obtained for all dyes. It is known that dyes with weak Stokes shifts present minimal conformational reorganization between the ground and excited state [43]. Our results showed that the spectral properties of the derivatives D1-D1.7 are weakly affected by these structural changes.

3.4. The Life Time of the Singlet Excited State (τ). The first excited state (S_1) to the ground--state (S_0) decay step is extremely important for injecting the excited electron into the conduction band minimum (CBM) of the TiO_2 semiconductor. Thus, the lifetime (τ) of the excited state is an extremely crucial parameter for evaluating the charge transfer efficiency [44]. A dye sensitizer having an excited state with a longer τ value is expected to facilitate the charge transfer [45]. In Table 4 are listed the decay time (τ/nm) of the derivatives. They are obtained using

$$\tau = \frac{1.499}{(E_{em})^2 f}, \quad (1)$$

where E_{em} is the emission energy in cm^{-1} and f is the oscillator strength of the transition state [46]. As Table 4 shows, apart from D1.3 and D1.4, the τ values for all the derivatives are much longer than that for the parent D1. They increase in the order D1<D1.2<D1.1<D1.5D1.7<D1.6. Therefore, generally the introduction of the electron withdrawing, apart

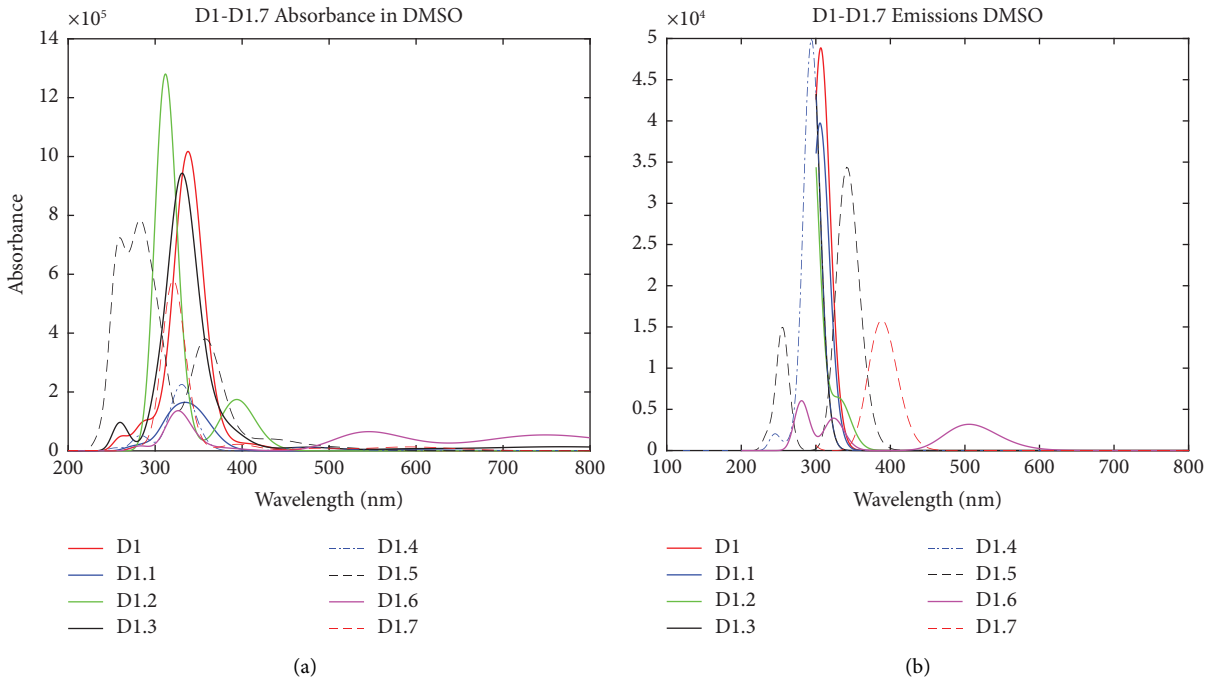

Figure 4: (a) Absorption and (b) emission spectra of the DMSO-solvated dyes (D1-D1.7) were simulated at the TD-B3LYP/6-311++G** level of theory.

Table 3: The calculated HOMO (eV), LUMO (eV), bandgap (ΔE/eV), absorption wavelengths (λ_{max}/nm), oscillator strengths (f), light harvesting efficiencies (LHE), and electronic transition assignments of the gas-phase D1-D1.7 derivatives using B3LYP/6-311++G**.

Dye	HOMO	LUMO	ΔE	λ_{max}	f	LHE	Major transition assignment
D1	−5.759	−1.165	4.594	290	0.530	0.705	HOMO- > LUMO (97%)
D1.1	−5.624	−0.993	4.631	287	0.400	0.602	HOMO- > LUMO (91%)
D1.2	−5.227	−0.771	4.456	282	0.171	0.326	H-1- > LUMO (48%), H-1- > L+1 (46%)
D1.3	−5.870	−1.078	4.792	275	0.412	0.613	HOMO- > LUMO (77%)
D1.4	−5.310	−1.894	3.415	300	0.406	0.607	HOMO- > LUMO (92%)
D1.5	−6.709	−2.392	4.317	305	0.311	0.512	HOMO- > LUMO (72%)
D1.6	−6.691	−3.232	3.459	435	0.024	0.055	HOMO- > LUMO (99%)
D1.7	−6.599	−2.315	4.284	244	0.145	0.284	H1>L+1(60%), H3>LUMO(28%),

Table 4: The calculated excitation energy (E), absorption wavelengths (λ_{max}), emission wavelength (λ_{em}), emission oscillator strength (f), light harvesting efficiency (LHE), excited-state lifetime (τ), and Stokes shift (SS) of dye D1 and its derivatives (D1.1-D1.7) in a DMSO solvent medium. They were calculated by using the TD-B3LYP/6-311++G** level of theory.

Dyes	HOMO	LUMO	EΔ	E (cm^{-1})	λ_{abs}(nm)	λ_{em}(nm)	f	LHE	τ(ns)	Stokes shift (SS)
D1	−5.764	−1.423	4.341	31475	306	318	0.671	0.787	2.3	12
D1.1	−5.762	−1.669	4.093	31775	305	315	0.546	0.715	2.7	10
D1.2	−5.791	−1.655	4.136	31876	293	314	0.577	0.735	2.6	21
D1.3	−5.707	−1.749	3.958	32925	294	304	0.626	0.763	2.2	10
D1.4	−6.088	−1.541	4.547	32817	294	305	0.688	0.795	2.0	11
D1.5	−6.341	−2.425	3.916	28435	342	352	0.454	0.648	4.1	10
D1.6	−6.314	−3.300	3.014	30797	280	325	0.080	0.168	19.7	45
D1.7	−6.091	−2.383	3.708	25339	388	395	0.192	0.357	12.2	7

from F atoms, or donating groups into DMABA, increases the lifetime of the excited state, expedites the energy transfer, and boosts the efficacy of DSSCs. Accordingly, the derivatives D1.6, D1.7, and D1.5, acquiring NO_2, CH_3 with CN, and CN groups, respectively, display substantially dynamic charge transfer and electron admission to the conduction band minimum of the TiO_2 semiconductor substrate. In addition, these three dyes could hinder the charge recombination process and boost the performance of DSSCs in comparison to D1. It is worth noting that the excited states of

derivatives, in the more polar solvent (DMSO), live longer compared to the less polar ones [47].

3.5. The Overall Performance. The power conversion efficiency (PCE) of DSSCs is investigated by the short-circuit current density (J_{SC}), open-circuit photovoltage (V_{OC}), and fill factor (FF) values, as well as the intensity of the incident light (P_{IN}). It is estimated by applying Equation (2) [48]:

$$\text{PCE} = \frac{1}{P_{\text{IN}}}\left(\text{FF} \times V_{\text{OC}} \times J_{\text{SC}}\right), \tag{2}$$

where FF is the ratio of the maximum power of the DSSC and the product of V_{OC}, J_{SC}, and P_{IN} [49]. As (2) shows, the impact of the electron withdrawing or donating groups on the product of V_{OC} and J_{SC} should be optimized to enhance the performance. V_{OC} can be computed by applying (3) [50],

$$V_{\text{OC}} = \frac{E_{\text{CB}}}{q} + \frac{k_B T}{q} ln\left[\frac{n_C}{N_{\text{CB}}}\right] - \frac{E_{\text{redox}}}{q}, \tag{3}$$

where k_BT is the thermal energy, q is the unit charge, and n_C is the number of electrons in the conduction band, N_{CB} is the conduction band attainable density of states, and E_{redox} is the electrolyte oxidation potential. V_{OC} is computed as an energy difference between the conduction band minimum of the TiO_2 semiconductor and the iodide/triiodide (I^-/I_3^-) electrolyte redox potential, which is assumed to be constant.

It is known that the value of J_{SC} in a DSSC can be computed by applying (4) [51]

$$J_{\text{SC}} = \int LHE(\lambda)\Phi_{\text{inject}}\eta_{\text{collect}}d\lambda, \tag{4}$$

where LHE denotes the light-harvesting efficiency with respect to a given wavelength (λ_{max}), Φ_{inject} gives the electron insertion efficacy, and $\eta_{collect}$ is related to the charge collection performance. In our proposed DSSCs, the electrode (I^-/I_3^-) is kept constant while the dye sensitizers are varied. Accordingly, $\eta_{collect}$ turns out to be a constant.

However, LHE(λ) can be estimated by (5) [52]:

$$\text{LHE}(\lambda) = 1 - 10^{-f}, \tag{5}$$

where f denotes the oscillator strength of the absorption wavelength (λ_{max}). It is known that the LHE and the free energy for electron injection (ΔG_{inject}) are the two important elements that impact J_{SC}. The values of LHE of the elected DMABA derivatives should be high to maximize the performance of the DSSCs. Higher oscillator strengths enhance the light harvesting efficiencies and maximize the overlap with the solar light, especially over the whole UV–visible spectral region. The light harvesting efficiencies (LHE) using TD-B3LYP/6-311++G** listed in Table 4 of the different DMSO-solvated DMABA derivatives (D1.1-D1.7) range between 0.168 and 0.795, indicating that these derivatives provide different photocurrent performances. J_{SC} can also be increased through enhancing the electron injection free energy (ΔG_{inject}) which can be computed by Equation (6) [53]

$$\Delta G_{\text{inject}} = E_{\text{OX}}^{\text{dye*}} - E_{\text{CB}}^{\text{TiO}_2}, \tag{6}$$

where $E_{CB}^{TiO_2}$ denotes the reduction potential energy level of the TiO_2 conduction band and E_{OX}^{dye*} gives the oxidation potential energy of the excited state DMABA derivatives, and $E_{CB}^{TiO_2}$ which can be estimated by (7) [54–56]:

$$E_{OX}^{dye*} = E_{OX}^{dye} - E, \tag{7}$$

where E_{OX}^{dye} denotes the ground-state energy of the DMABA derivatives in the oxidation potential energy, while E is the lowest vertical electronic excitation energy, related to λ_{max}.

As registered in Table 5, all the elected DMABA derivatives give negative ΔG_{inject} values, where D1.2 gives the most negative value; while D1.7 shows the least negative one. In addition, the electron donating groups CH_3, OH, and NH_2 represented by D1.1, D1,2, and D1.3, respectively, yield more negative values compared to that of the parent D1; while the electron-withdrawing moieties F, CN, NO_2, and CN with CH_3 represented by D1.4, D1.5, D1.6, and D1.17, respectively, give less negative ones relative to that of their predecessor D1 (See Table 5). The absolute values of ΔG_{inject} for all DMABA derivatives understudy are much greater than the 0.2 eV threshold necessary for an efficient electron injection [57]. It is noteworthy that the large energy difference between the LUMOs of the DMABA derivatives and the CBM of TiO_2 of −4.0 eV is large enough to secure efficient electron injections (See Figure 5).

J_{SC} of the DSSC is affected by the regeneration efficiency (η_{reg}) of the DMABA derivatives, which can be computed from the regeneration force represented by ΔG_{reg} shown by (8) [58],

$$\Delta G_{\text{reg}} = E_{\text{redox}}^{\text{electrolyte}} - E_{\text{OX}}^{\text{dye}}. \tag{8}$$

Table 5 lists the computed values of ΔG_{reg} for the derivatives D1.1–D1.7 of 0.829, 0.717, 1.085, 1.289, 1.542, 1.514, and 1.286 eV, respectively. It is clear that D1.1 and D1.2 offer relatively smaller driving forces for dye regeneration, which may enhance η_{reg} compared with the parent D1 (0.965 eV). In particular, derivative D1.2 could present the fastest regeneration, promoting the DSSC efficacy. In addition, V_{OC} is computed as an energy difference between E_{LUMO} of the DMABA derivative and E_{CB} of the TiO_2 semiconductor [59]:

$$V_{\text{OC}} = E_{\text{LUMO}} - E_{\text{CB}}^{TiO_2}. \tag{9}$$

Our theoretical protocol has yielded V_{OC} values for the DMSO-solvated derivatives that spread between 0.699 and 2.931 eV (see Table 5). These values are quite appropriate for enabling efficacious electron injection into the LUMO of the carboxylate moiety as an electron acceptor. Thus, all the elected derivatives could be applied as sensitizers. This is because the carboxylate (COOH) acceptor group is quite propitious for electron injection from the dye into the CBM of the TiO_2 semiconductor, a situation that results in improved V_{OC} values. The derivative D1.2 characterized by the NH_2 moiety as an electron donating group, showed the highest V_{OC} value and hence could acquire an outstanding potential for application in DSSCs.

Table 5: The calculated band gap (ΔE), ground (E_{ox}^{dye}) and excited state (E_{ox}^{dye*}) oxidation potentials, vertical transition energy (λ_{max}^{ICT}), driving force for dye regeneration (ΔG_{reg}), electron injection efficiency (ΔG_{inject}), open circuit photovoltage (V_{OC}), and binding energy (E_b) of the dye D1 and its derivatives D1.1–D1.7 in a DMSO solvent medium. They were calculated by using the TD-B3LYP/6-311++G** level of theory.

Dyes	ΔE	E_{ox}^{dye}	λ_{max}^{ICT}	E_{ox}^{dye*}	ΔG_{reg}	ΔG_{injec}	V_{OC}	E_b
D1	4.341	5.765	4.055	1.718	0.965	−2.282	2.577	0.352
D1.1	4.093	5.629	4.068	1.569	0.829	−2.431	2.811	0.372
D1.2	4.136	5.517	4.235	1.283	0.717	−2.717	2.931	0.245
D1.3	3.958	5.885	4.220	1.669	1.085	−2.331	2.679	0.344
D1.4	4.547	6.089	4.220	1.870	1.289	−2.130	2.459	0.344
D1.5	3.916	6.342	3.639	2.703	1.542	−1.297	1.574	0.277
D1.6	3.014	6.314	4.431	1.893	1.514	−2.107	0.699	−1.418
D1.7	3.708	6.086	3.198	2.890	1.286	−1.110	1.615	0.503

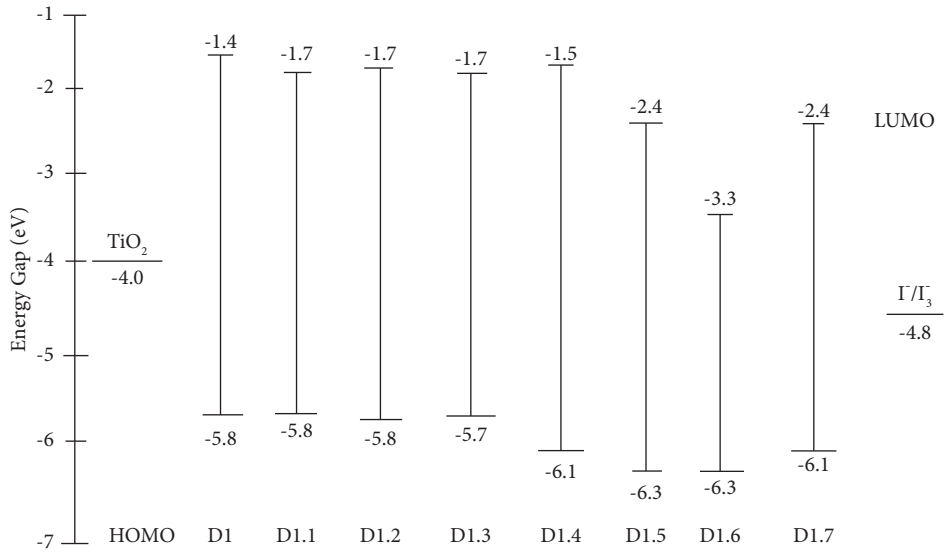

Figure 5: Schematic diagram of the HOMO-LUMO energy levels of the DMSO-solvated D1 and D1.1-D1.7 dyes were estimated by using the B3LYP/6-311++G** level of theory.

3.6. The Binding Energy (E_b). For a high power conversion efficiency (PCE), the electron-hole entities must be kept separate as positive and negative charges to avoid recombination as a result of the attractive Coulombic forces. To achieve this crucial process, the binding energy (E_b) should be overcome, i.e., the derivatives should have lower binding energy to yield high PCE values. The binding energy (E_b) could be computed by (10) [60, 61],

$$E_b = E_g - E_x = E_{H-L} - \lambda_{max}, \tag{10}$$

where E_g is the HOMO–LUMO energy gap and E_x is the optical energy, calculated with reference to λ_{max}. Table 5 lists the exciton computed binding energies for the parent D1 and its derivatives D1.1-D1.7. It reveals the lowest value for D1.6 compared with the remaining derivatives. These findings reconfirm that the derivative D1.6 characterized by the NO_2 group is the most preferable for fabricating DSSCs.

4. Conclusion

We attempted to explore the optimized geometry, electronic structure, and their related optical absorption and emission properties of eight D–π–A-type chromophores with different ortho or para electron withdrawing or donating moieties. Our findings demonstrate that the ortho electron donating NH_2, the meta electron withdrawing CN, and the ortho electron donating CH_3 with meta electron withdrawing CN groups applied in D1.2, D1.5, and D1.7, respectively, are favorable for implication in the D–π–A design. The coplanar environment of the dimethylamine donor, benzene ring, and carboxylate acceptor together with the ortho or meta groups boosts efficacious injection of electrons from the donor [$(CH_3)_2$N-] to the acceptor [--COOH] of the elected dyes. Our findings show that the electron- withdrawing or donating moieties implicated in D1.2, D1.5 and D1.7 have generated relatively strong absorptions for maintaining stable charge transfer pathways for prompt electron grouting and dye regeneration, first singlet excited-state lifetime, and exciton binding energy. In addition, the elected dyes D1.5, D1.6, and D1.7 show small HOMO-LUMO energy gaps and clear red shifts in absorption and emission, compared with the parent dye (D1). It could be concluded that the elected dyes D1.2, D1.5, D1.6, and D1.7 are more favorable nominees for applications in relatively potent organic DSSCs.

Data Availability

The authors confirm that the data supporting the findings of this study are available within the article and the accompanying materials.

Conflicts of Interest

The authors declare that they have no conflicts of interest.

Authors' Contributions

O.I.O. planned the research. S.A.E. and S.G.A. provided the necessary literature, and M.A.H. performed some calculations and proofread the manuscript. M.Y.A reset of the calculation, analyzed the results, and wrote the first version of the manuscript.

Acknowledgments

This work was supported by the Deanship of Scientific Research (DSR) King Abdulaziz University, Jeddah, under grant no. (G:84–130-1441). The authors, therefore, gratefully acknowledge with thanks the DSR's technical and financial support. The authors are highly indebted to the High-Performance Computing (HPC) Center at King Abdulaziz University for their technical support.

Supplementary Materials

Supplemental Table 1 shows electronic absorption spectra of gas-phase free *p*-N,N-(Dimethylamino) benzoic acid. Supplemental Table 2 lists the total energy, number of imaginary frequencies, and Standard Orientation of 4-DMABA. Supplemental Table 3 lists the total energy, number of imaginary frequencies, and Standard Orientation of Ti^{+4}-DMABA. Supplemental Tables 4–10 list the total energies, number of imaginary frequencies, and Standard Orientations of D1.1-D1.7 substrates. Supplemental Figure 1 shows the electronic absorption spectrum of the free 4-(dimethylamino) benzoic acid using the B3LYB/6–311++ G^{**} level of theory. Supplemental Figure 2 shows the electronic absorption spectrum of the free 4-(dimethylamino) benzoic acid using the PBEPBE/6–311++ G^{**} level of theory. (*Supplementary Materials*)

References

[1] N. Shamsul, S. Kamarudin, N. Rahman, N. Kofli, and N. T. Kofli, "An overview on the production of bio-methanol as potential renewable energy," *Renewable and Sustainable Energy Reviews*, vol. 33, pp. 578–588, 2014.

[2] J. Hansen, M. Sato, P. Kharecha, G. Russell, D. W. Lea, and M. Siddall, "Climate change and trace gases," *Philosophical Transactions of the Royal Society A: Mathematical, Physical and Engineering Sciences*, vol. 365, no. 1856, pp. 1925–1954, 2007.

[3] L. M. Gonçalves, V. de Zea Bermudez, H. A. Ribeiro, and A. M. Mendes, "Dye-sensitized solar cells a safe bet for the future," *Energy and Environmental Science*, vol. 1, no. 6, p. 655, 2008.

[4] A. A. F. Husain, W. Z. W. Hasan, S. Shafie, M. N. Hamidon, and S. S. Pandey, "A review of transparent solar photovoltaic technologies," *Renewable and Sustainable Energy Reviews*, vol. 94, pp. 779–791, 2018.

[5] A. Demirbaş, "Global renewable energy resources," *Energy Sources, Part A: Recovery*, vol. 28, no. 8, pp. 779–792, 2006.

[6] P. Roy, D. Kim, I. Paramasivam, and P. Schmuki, "Improved efficiency of TiO_2 nanotubes in dye sensitized solar cells by decoration with TiO_2 nanoparticles," *Electrochemistry Communications*, vol. 11, no. 5, pp. 1001–1004, 2009.

[7] T. Daeneke, Y. Uemura, N. W. Duffy et al., "Aqueous dye-sensitized solar cell electrolytes based on the ferricyanide–ferrocyanide redox couple," *Advanced Materials*, vol. 24, no. 9, pp. 1222–1225, 2012.

[8] C. Wang, F. Meng, M. Wu et al., "A low-cost bio-inspired integrated carbon counter electrode for high conversion efficiency dye-sensitized solar cells," *Physical Chemistry Chemical Physics*, vol. 15, no. 34, 2013.

[9] X. Li, P. Song, D. Zhao, and Y. Li, "Theoretical investigation on photophysical properties of triphenylamine and coumarin dyes," *Materials*, vol. 13, no. 21, 2020.

[10] W. R. Duncan and O. V. Prezhdo, "Temperature independence of the photoinduced electron injection in dye-sensitized TiO_2 rationalized by *ab initio* time-domain density functional theory," *Journal of the American Chemical Society*, vol. 130, no. 30, pp. 9756–9762, 2008.

[11] C. L. Wang, J. Wang, F. Q. Bai, J. Chen, and H. X. Zhang, "Molecular design of organic dyes with diketopyrrolopyrrole for dye-sensitized solar cell a theoretical approach," *International Journal of Quantum Chemistry*, vol. 114, no. 9, pp. 560–567, 2014.

[12] H.-Bo Guo, F. He, B. Gu, L. Liang, and J. C. Smith, "Time-dependent density functional theory assessment of UV absorption of benzoic acid derivatives," *Journal of Physical Chemistry A*, vol. 116, no. 48, pp. 11870–11879, 2012.

[13] L. W. Peng, M. Dantus, A. H. Zewail, K. Kemnitz, J. M. Hicks, and K. B Eisenthal, "Stepwise solvation of the intramolecular-charge-transfer molecule *p*-(dimethylamino)benzonitrile," *Journal of Physical Chemistry*, vol. 91, no. 24, pp. 6162–6167, 1987.

[14] T. F. Lai and R. E. Marsh, "The crystal structure of p-aminobenzoic acid," *Acta Crystallographica*, vol. 22, no. 6, pp. 885–893, 1967.

[15] M. J. Frisch, G. W. Trucks, H. B. Schlegel et al., *Gaussian 09*, Gaussian Inc, Wallingford, 2009.

[16] R. Dennington, T. Keith, and J. Millam, *GaussView, Version 5.0. 9*, Shawnee Mission Semichem Inc, Shawnee, KS, 2009.

[17] C. Lee, W. Yang, and R. G. Parr, "Development of the Colle-Salvetti correlation-energy formula into a functional of the electron density," *Physical Review B: Condensed Matter*, vol. 37, no. 2, pp. 785–789, 1988.

[18] T. Yanai, D. P. Tew, and N. C. Handy, "A new hybrid exchange–correlation functional using the Coulomb-attenuating method (CAM-B3LYP)," *Chemical Physics Letters*, vol. 393, no. 1-3, 2004.

[19] J. P. Perdew, M. Ernzerhof, and K. Burke, "Rationale for mixing exact exchange with density functional approximations," *The Journal of Chemical Physics*, vol. 105, no. 22, pp. 9982–9985, 1996.

[20] J.-D. Chai and M. Head-Gordon, "Long-range corrected hybrid density functionals with damped atom-atom dispersion corrections," *Physical Chemistry Chemical Physics*, vol. 10, no. 44, pp. 6615–6620, 2008.

[21] E. Runge and E. K. U. Gross, "Density-functional theory for time-dependent systems," *Physical Review Letters*, vol. 52, no. 12, pp. 997–1000, 1984.

[22] S. Lenoid, "Chemissian v3.3," 2012, https://www.chemissian.com/.

[23] M. J. Frisch, J. A. Pople, and J. S. Binkley, "Self-consistent molecular orbital methods 25. Supplementary functions for Gaussian basis sets," *The Journal of Chemical Physics*, vol. 80, no. 7, pp. 3265–3269, 1984.

[24] J. Tomasi, B. Mennucci, and R. Cammi, "Quantum mechanical continuum solvation models," *Chemical Reviews*, vol. 105, no. 8, pp. 2999–3094, 2005.

[25] L. Leiserowitz, "Molecular packing modes. Carboxylic acids," *Acta Crystallographica Section B Structural Crystallography and Crystal Chemistry*, vol. 32, no. 3, pp. 775–802, 1976.

[26] F. H. Allen, O. Kennard, D. G. Watson, L. Brammer, A. G. Orpen, and R. Taylor, "Tables of bond lengths determined by X-ray and neutron diffraction. Part 1. Bond lengths in organic compounds," *Journal of the Chemical Society Perkin Transactions*, vol. II, no. 12, pp. S1–S19, 1987.

[27] R. Pearson Jr. and F. J. Lovas, "Microwave spectrum and molecular structure of methylenimine (CH_2NH)," *The Journal of Chemical Physics*, vol. 66, no. 9, 1977.

[28] M. D. Harmony, "The equilibrium carbon–carbon single-bond length in ethane," *The Journal of Chemical Physics*, vol. 93, no. 10, pp. 7522-7523, 1990.

[29] N. C. Craig, P. Groner, and D. C. McKean, "Equilibrium structures for butadiene and ethylene: compelling evidence for Π-electron delocalization in butadiene," *The Journal of Physical Chemistry A*, vol. 110, no. 23, pp. 7461–7469, 2006.

[30] T. Hökelek, H. Dal, B. Tercan, O. Aybirdi, and H. Necefoğlu, "Diaqua-bis[4-(dimethyl-amino) benzoato] (iso-nicotinamide) zinc (II)," *Acta Crystallographica, Section E: Structure Reports Online*, vol. 65, no. 6, 2009.

[31] D. F. Perepichka and M. R. Bryce, "Molecules with exceptionally small HOMO–LUMO gaps," *Angewandte Chemie International Edition*, vol. 44, no. 34, pp. 5370–5373, 2005.

[32] R. L. Carroll and C. B. Gorman, "The genesis of molecular electronics," *Angewandte Chemie International Edition*, vol. 41, pp. 4378–4400, 2002.

[33] D. Kosenkov and L. V. Slipchenko, "Solvent effects on the electronic transitions of p-nitroaniline a QM/EFP study," *Journal of Physical Chemistry A*, vol. 115, no. 4, pp. 392–401, 2011.

[34] S. G. Aziz, O. I. Osman, S. A. Elroby, W. M. I. Hassan, A. Jedidi, and R. H. Hilal, "Proton-coupled electron transfer in dye-sensitized solar cells: a theoretical perspective," *Structural Chemistry*, vol. 29, no. 4, pp. 983–997, 2018.

[35] T. Fransson and A. Dreuw, "Simulating X-ray emission spectroscopy with algebraic diagrammatic construction schemes for the polarization propagator," *Journal of Chemical Theory and Computation*, vol. 15, no. 1, pp. 546–556, 2018.

[36] J. J. Apperloo, R. A. J. Janssen, P. R. L. Malenfant, L. Groenendaal, and J. M. J. Fréchet, "Redox states of well-defined π-conjugated oligothiophenes functionalized with poly(benzyl ether) dendrons," *Journal of the American Chemical Society*, vol. 122, no. 29, 2000.

[37] P. M. Beaujuge, C. M. Amb, and J. R. Reynolds, "Spectral engineering in π-conjugated polymers with intramolecular Donor–Acceptor interactions," *Accounts of Chemical Research*, vol. 43, no. 11, pp. 1396–1407, 2010.

[38] J. Choi, K. Yeo, M. Yoon, S. J. Lee, and K. Kim, "Photoinduced intramolecular charge-transfer state of p-dimethylamino-benzoic acid in CdS and TiO_2 colloid solutions," *Journal of Photochemistry and Photobiology A: Chemistry*, vol. 132, no. 1-2, pp. 105–114, 2000.

[39] D. Jacquemin, J. Preat, E. A. Perpète et al., "Absorption spectra of azobenzenes simulated with time-dependent density functional theory," *International Journal of Quantum Chemistry*, vol. 111, no. 15, pp. 4224–4240, 2011.

[40] J. M. Herbert and M. Head-Gordon, "Calculation of electron detachment energies for water cluster Anions: an appraisal of electronic structure methods, with application to $(H2O)_{20}$- and $(H2O)_{24}$-," *Journal of Physical Chemistry A*, vol. 109, no. 23, pp. 5217–5229, 2005.

[41] Z. M. E. Fahim, S. M. Bouzzine, A. A. Youssef, M. Bouachrine, and M. Hamidi, "Ground state geometries, UV/vis absorption spectra and charge transfer properties of triphenylamine-thiophenes based dyes for DSSCs a TD-DFT benchmark study," *Computational and Theoretical Chemistry*, vol. 1125, pp. 39–48, 2018.

[42] V. Mollica Nardo, G. Cassone, R. C. Ponterio et al., "Electric-field-induced effects on the dipole moment and vibrational modes of the centrosymmetric indigo molecule," *Journal of Physical Chemistry A*, vol. 124, no. 51, 2020.

[43] L. X. Chen, G. Jennings, T. Liu et al., "Rapid excited-state structural reorganization captured by pulsed X-rays," *Journal of the American Chemical Society*, vol. 124, no. 36, pp. 10861–10867, 2002.

[44] W. Hu, P. Yu, Z. Zhang, W. Shen, M. Li, and R. He, "Theoretical study of YD2-o-C8-based derivatives as promising sensitizers for dye-sensitized solar cells," *Journal of Materials Science*, vol. 52, no. 3, pp. 1235–1245, 2017.

[45] K. Chaitanya, X. H. Ju, and B. M. Heron, "Theoretical study on the light harvesting efficiency of zinc porphyrin sensitizers for DSSCs," *RSC Advances*, vol. 4, no. 51, pp. 26621–26634, 2014.

[46] M. Li, L. Kou, L. Diao et al., "Theoretical study of WS-9-based organic sensitizers for unusual Vis/NIR absorption and highly efficient dye-sensitized solar cells," *Journal of Physical Chemistry C*, vol. 119, no. 18, pp. 9782–9790, 2015.

[47] D. Patra, N. N. Malaeb, M. J. Haddadin, and M. J. Kurth, "Influence of substituent and solvent on the radiative process of singlet excited states of novel cyclic azacyanine derivatives," *Journal of Fluorescence*, vol. 22, no. 2, pp. 707–717, 2012.

[48] M. R. Narayan, "Review dye sensitized solar cells based on natural photosensitizers," *Renewable and Sustainable Energy Reviews*, vol. 16, pp. 208–215, 2011.

[49] J. Preat, D. Jacquemin, and E. A. Perpete, "Towards new efficient dye-sensitised solar cells," *Energy and Environmental Science*, vol. 3, no. 7, pp. 891–904, 2010.

[50] T. Marinado, K. Nonomura, J. Nissfolk et al., "How the nature of triphenylaminepolyene dyes in dye-sensitized solar cells affects the open-circuit voltage and electron lifetimes," *Langmuir*, vol. 26, no. 4, pp. 2592–2598, 2010.

[51] J. Zhang, H. B. Li, S. L. Sun, Y. Geng, Y. Wu, and Z. M. Su, "Density functional theory characterization and design of high performance diarylamine-fluorene dyes with different π spacers for dye-sensitized solar cells," *Journal of Materials Chemistry*, vol. 22, no. 2, pp. 568–576, 2012.

[52] Z. L. Zhang, L. Y. Zou, A. M. Ren et al., "Theoretical studies on the electronic structures and optical properties of star-shaped triazatruxene/heterofluorene co-polymers," *Dyes and Pigments*, vol. 96, no. 2, pp. 349–363, 2013.

[53] R. Katoh, A. Furube, T. Yoshihara et al., "Efficiencies of electron injection from excited N3 dye into nanocrystalline semiconductor (ZrO2, TiO_2, ZnO, Nb_2O_5, SnO_2, In_2O_3) films," *Journal of Physical Chemistry B*, vol. 108, no. 15, pp. 4818–4822, 2004.

[54] J. Preat, D. Jacquemin, C. Michaux, and E. A. Perpète, "Improvement of the efficiency of thiophene-bridged compounds for dye sensitized solar cells," *Chemical Physics*, vol. 376, no. 1-3, pp. 56–68, 2010.

[55] J. Zhang, Y. H. Kan, H. B. Li et al., "How to design proper π-spacer order of the D–π–A dyes for DSSCs? A density functional response," *Dyes and Pigments*, vol. 95, no. 2, pp. 313–321, 2012.

[56] W. L. Ding, D. M. Wang, Z. Y. Geng, X. L. Zhao, and W. B. Xu, "Density functional theory characterization and verification of high-performance indoline dyes with D–A–π–A architecture for dye-sensitized solar cells," *Dyes and Pigments*, vol. 98, no. 1, pp. 125–135, 2013.

[57] A. Islam, H. Sugihara, and H. Arakawa, "Molecular design of ruthenium (II) polypyridyl photosensitizers for efficient nanocrystalline TiO_2 solar cells," *Journal of Photochemistry and Photobiology A: Chemistry*, vol. 158, no. 2-3, pp. 131–138, 2003.

[58] T. Daeneke, A. J. Mozer, Y. Uemura et al., "Dye regeneration kinetics in dye-sensitized solar cells," *Journal of the American Chemical Society*, vol. 134, no. 41, pp. 16925–16928, 2012.

[59] W. Sang-aroon, S. Saekow, and V. A. Amornkitbamrung, "Density functional theory study on the electronic structure of Monascus dyes as photosensitizer for dye-sensitized solar cells," *Journal of Photochemistry and Photobiology A: Chemistry*, vol. 236, pp. 35–40, 2012.

[60] Y. Li, T. Pullerits, M. Zhao, and M. Sun, "Theoretical characterization of the $PC_{60}BM$: PDDTT model for an organic solar cell," *Journal of Physical Chemistry C*, vol. 115, no. 44, pp. 21865–21873, 2011.

[61] R. Nithya and K. Senthilkumar, "Theoretical studies on the quinoidal thiophene based dyes for dye sensitized solar cell and NLO applications," *Physical Chemistry Chemical Physics*, vol. 16, no. 39, pp. 21496–21505, 2014.